applied sciences

MDPI

Article

Tensile Properties and Tensile Failure Criteria of Layered Rocks

Min Gao [1,2,3], Zhengzhao Liang [2,*], Shanpo Jia [3] and Jiuqun Zou [1]

1 State Key Laboratory of Mining Response and Disaster Prevention and Control in Deep Coal Mines, Anhui University of Science and Technology, Huainan 232001, China; gaomin@aust.edu.cn (M.G.); 2020136@aust.edu.cn (J.Z.)
2 State Key Laboratory of Coastal and Offshore Engineering, Dalian University of Technology, Dalian 116024, China
3 Institute of Unconventional Oil & Gas, Northeast Petroleum University, Daqing 163318, China; jiashanporsm@163.com
* Correspondence: liangzz@dlut.edu.cn

Abstract: Rocks are less resistant to tension than to compression or shear. Tension cracks commonly initiate compression or shear failure. The mechanical behavior of layered rocks under compression has been studied extensively, whereas the tensile behavior still remains uncertain. In this paper, we study the effect of layer orientation on the strength and failure patterns of layered rocks under direct and indirect tension through experimental and numerical testing (RFPA^{2D}: numerical software of Rock Failure Process Analysis). The results suggest that the dip angle of the bedding planes significantly affects the tensile strength, failure patterns, and progressive deformation of layered rocks. The failure modes of the layered specimens indicate that the tensile strength obtained by the Brazilian disc test is not as accurate as that obtained by the direct tension test. Therefore, the modified Single Plane of Weakness (MSPW) failure criterion is proposed to predict the tensile strength of the layered rocks based on the failure modes of direct tension. The analytical predictions of the MSPW failure criterion agrees closely with the experimental and numerical results. In rock engineering, the MSPW failure criterion can conveniently predict the tensile strength and reflect the failure modes of layered rocks (such as shale, slate, and layered sandstone) with satisfactory accuracy.

Keywords: layered rocks; anisotropy; failure mode; tension test; tensile failure criterion

check for updates

Citation: Gao, M.; Liang, Z.; Jia, S.; Zou, J. Tensile Properties and Tensile Failure Criteria of Layered Rocks. *Appl. Sci.* **2022**, *12*, 6063. https://doi.org/10.3390/app12126063

Academic Editor: Ricardo Castedo

Received: 22 May 2022
Accepted: 14 June 2022
Published: 15 June 2022

1. Introduction

Many types of rock mass, such as shale, slate, and sandstone, exhibit inherent anisotropic properties [1–4]. The uniaxial compressive and tensile strength of layered rocks are crucial parameters to consider at the design and construction stage of geotechnical structures such as tunnels, slopes, and other underground engineering projects. They are also vitally important for the development of unconventional oil and gas, such as shale gas [5,6]. However, only the anisotropic compressive (or shear) strength has been extensively studied from experimental, theoretical, and numerical points of view [7–11], but the anisotropic tensile strength still needs to be further investigated because tensile failure is extremely important in rock engineering. In fact, the tensile strength of layered rocks was previously assumed to be nil in many engineering applications. There are situations, however, where such an assumption is not safe. As a result, the tensile failure of rock and the resulting instability can lead to serious disasters, such as rock burst in hydropower caverns, landslide, dam break, and so on [12]. Therefore, understanding the tensile properties of layered rocks is extremely important to assess the stability of geotechnical and petroleum engineering projects.

There are two main methods to assess the tensile strength of layered rocks, including the direct uniaxial tension test and the indirect tension test, such as the Brazilian disc test (BDT) and other indirect testing methods [13]. The Brazilian disc test was officially proposed by the International Society for Rock Mechanics [14] as a suggested method for determining the tensile strength of rock materials. The Brazilian disc test is the most commonly adopted method to determine the indirect tensile strength of rock materials [15–23]. However, during the Brazilian test, a small eccentricity of the axial load may cause large non-uniformities of stress in specimens [24], or stress concentrations may be induced by caps. For transversely isotropic rock masses, failure under the Brazilian test is not necessarily a pure tensile failure; in some cases, it can even be pure shear failure, but it is often a combination of both tensile and shear failure [25–27]. Although these disadvantages are obviously present in the Brazilian test, it is still widely used in laboratory experimental and numerical studies to investigate the tensile properties of transversely isotropic rocks [28–34].

The direct tensile test, which is theoretically the simplest and most effective method for tensile strength determination, is in fact difficult to carry out in the laboratory [35–38]. Over the past few decades, the anisotropic tensile behavior of layered rocks has been studied by a few researchers through direct tension [39,40]. Some anisotropic tensile criteria were investigated to predict the tensile strength of layered rocks based on the direct tension test and analytical methods [41–43]. Ma et al. analyzed the anisotropic tension strength criteria of layered rocks and selected the best one to predict the fracture pressure of the inclined wells in layered formations [44,45]. Shang et al. investigated the anisotropic direct tensile behavior of laminated and transversely isotropic Midgley Grit sandstone using a particle-based discrete element method [46]. However, the tensile failure modes and failure mechanisms of layered rocks still need to be further studied. Furthermore, the failure criterion of the layered rocks under direct tension should be evaluated based on the failure modes.

In this work, numerical tests are undertaken to investigate the progressive failure and mechanical behavior of layered rocks under direct and indirect tension using a numerical code RFPA^{2D}, which was developed based on the finite element method, statistical theory, and damage mechanics [47]. The influence of layer orientation on tensile behavior is discussed. The main failure modes and failure mechanisms of layered rocks under direct and indirect tension are analyzed. The Single Plane of Weakness failure criterion is then modified based on the failure modes and failure mechanisms of direct tension. The modified SPW (MSPW) failure criterion has been verified by experimental and numerical results. The analytical predictions of the MSPW failure criterion agrees closely with the experimental and numerical results.

2. Experimental Study on Layered Rocks by the Brazilian Test

2.1. Test Equipment and Samples

Layered rock samples (shale in Figure 1) with different dip angles, θ (the angle between the bedding plane and the horizontal plane), as shown in Figure 2, were selected for the experiments. According to the method suggested by the International Society for Rock Mechanics (ISRM), the samples were carefully drilled from a large fresh shale block. They were machined into Brazilian disc cylinders (25 mm in thickness and 50 mm in diameter) with seven different dip angels ($0°, 15°, 30°, 45°, 60°, 75°, 90°$). These samples are displayed in Figure 1. The experiments were performed using a Rock Mechanics Testing System (RMT-150C). The axial displacement loading mode was selected, with a controlled rate of 0.0005 mm/s until the failure of the tested shale sample. A photograph and a schematic diagram of the experimental setup is presented in Figure 2.

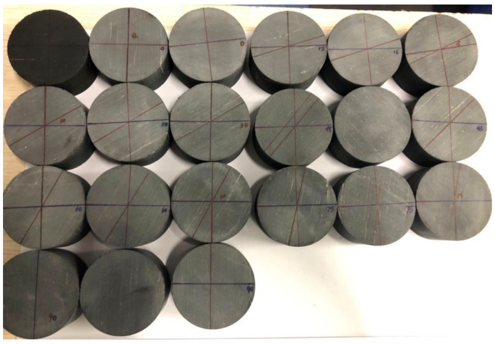

Figure 1. Layered shale samples with different dip angles under the Brazilian test.

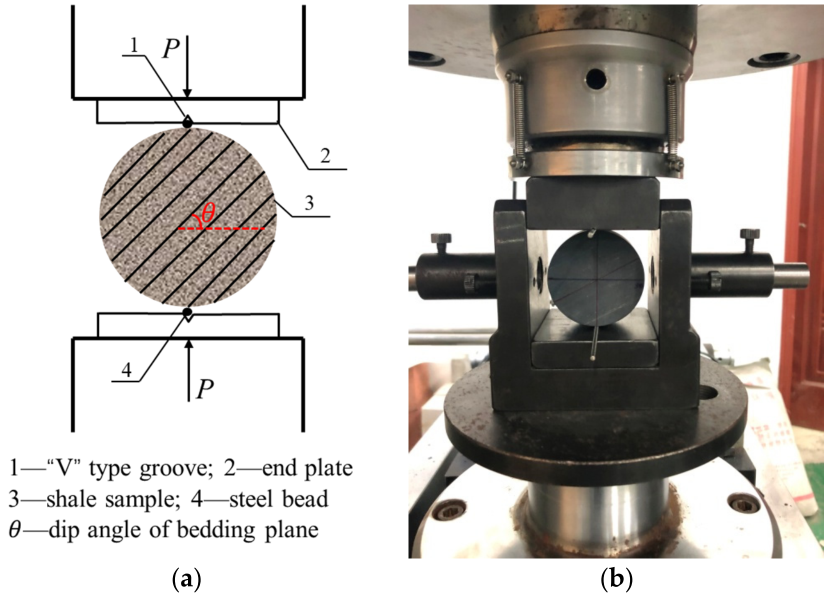

Figure 2. Loading schematic of the layered shale Brazilian test. (**a**) Loading schematic diagram; (**b**) Photograph of experimental setup.

According to the theory of the Brazilian disc test, the tensile strength of rock samples can be expressed as (negative sign represents tensile stress):

$$\sigma_t = -\frac{2P_t}{\pi D t} \tag{1}$$

where P_t is the failure load of the rock sample, D is the diameter of the rock sample, and t is the thickness of the rock sample.

2.2. Failure Mode of the Shale Samples

Figure 3 shows the typical failure modes of layered shale samples with different dip angles under the Brazilian test. When the dip angle of the sample was 0°, the shale sample almost cracked along the center line of the disc. When the dip angle of the shale sample increases to 30°, the shale sample first fractured near the loading end, and then cracked along the bedding plane. With the increasing dip angle of the samples, the shale samples almost presented shear failure along the bedding plane. The failure mode of the shale sample with a dip angle of 90° was similar to the sample at 0°. The failure modes of shale samples with different dip angles can be summarized as follows: splitting failure along the center line of the disc, composite failure with tensile and shear cracks, and shear failure along the bedding plane. The failure modes of the shale samples show anisotropic characteristics, and also indicate that only the shale samples with dip angles of 0° and 90°

experience splitting failure along the center line of the disc, which satisfies the assumption of Equation (1). In another words, the tensile strength of the shale samples with different dip angles obtained by the Brazilian test are not quite accurate, except for the shale samples with dip angles of 0° and 90°.

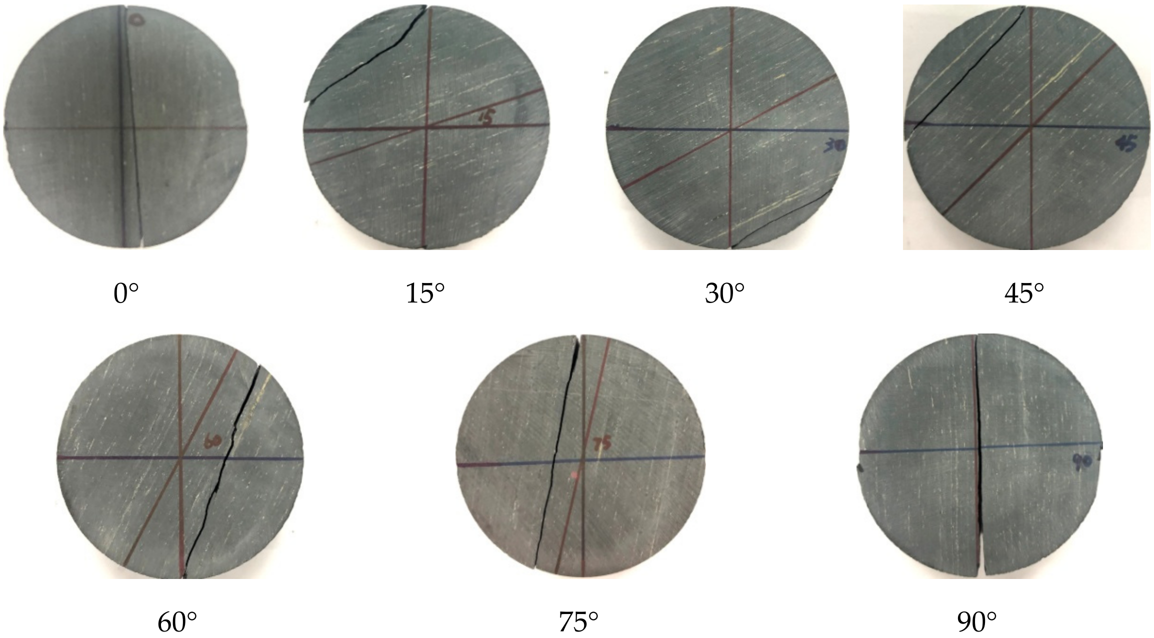

Figure 3. Typical failure modes of layered shale under the Brazilian test.

2.3. Tensile Strength of the Shale Samples

Figure 4 shows the variable relationship between the tensile strength of shale samples and the dip angles of the bedding plane. Figure 4 demonstrated that the tensile strength of the shale samples obviously represents anisotropic characteristics. By increasing the dip angle of the bedding plane, the tensile strength of the shale sample decreases. The tensile strength of the shale sample with a dip angle of 0° is the largest. This tensile strength can be considered as the tensile strength of the rock matrix, because the sample is cracked along the center line of the disc. Meanwhile, the tensile strength of the shale sample with a dip angle of 90° is the smallest. The failure mode of the sample is closer to that of the sample with a dip angle of 0°. However, the tensile strength of the sample with a dip angle of 0° is regarded as the tensile strength of the bedding plane. In Figure 4, it can be clearly seen that the tensile strength of the shale samples changes significantly when the dip angle of the bedding plane increases from 0° to 15°. Relatively, the tensile strength of the shale samples changes gradually when the dip angle of the bedding plane increases from 15° to 75°. The variation of the tensile strength of the shale samples is closely related to the failure modes, as analyzed above.

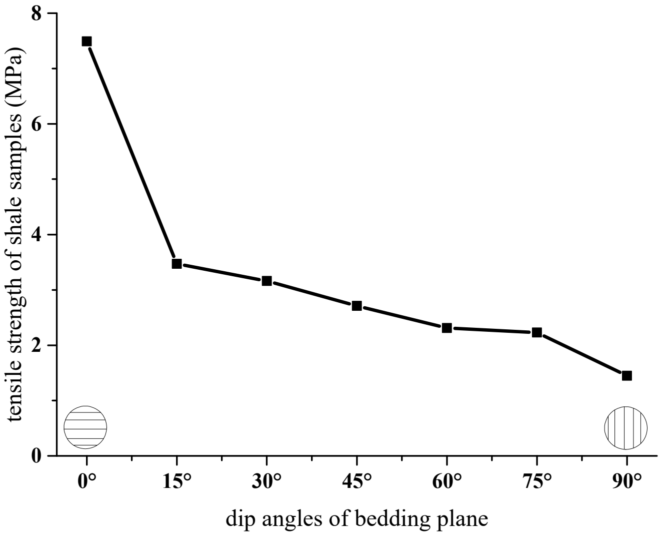

Figure 4. Average tensile strength of layered shale versus dip angles of the bedding plane.

3. Numerical Study of Layered Rocks

3.1. Description of the Numerical Code

The RFPA^{2D} code was developed by considering the deformation of an elastic material containing an initial random distribution of micro-features to simulate the progressive failure, including the simulation of the failure process, failure-induced seismic events, and failure-induced stress redistribution. There are two main features of RFPA^{2D} that are different from the traditional finite element method: (a) The heterogeneity of rock properties is introduced into the model; the RFPA^{2D} code can simulate the non-linear deformability of a quasi-brittle behavior with an ideal brittle constitutive law for the local material. (b) A simple elastic–brittle–plastic model is implemented in the RFPA^{2D} code. The element maintains linear deformation before the elemental stresses satisfy the failure criterion. The element has a residual strength after failure, and the stiffness of the element will decrease gradually. In this manner, the code can simulate strain-softening and discontinuous mechanical problems in a continuum mechanics mode. Both maximal tensile stress criterion and maximal tensile strain criterion are adopted in the model. The maximal tensile stress criterion is used to predict the brittle failure from the elastic stage to the residual deformation stage, and the maximal tensile strain criterion is applied to predict when the element loses its carrying capacity completely.

For heterogeneity, the material properties for elements are randomly distributed throughout the specimen by following a Weibull distribution:

$$\varphi = \frac{m}{\sigma_0}\left(\frac{\sigma}{\sigma_0}\right)^{m-1} exp\left[-\left(\frac{\sigma}{\sigma_0}\right)^{m}\right] \quad (2)$$

where, φ represents the strength of the elements distribution rule, σ is the element strength, and σ_0 is the mean strength of all the elements for the specimen. For an elastic modulus, the same distribution is used. We define m as the homogeneity index of the rock. A user-friendly pre- and post-processor is integrated to generate the finite element mesh and prepare the input data. The RFPA^{2D} code can not only simulate the initiation of cracks, but can also model the crack propagation, coalescence, and interaction between multi-cracks. Details of the RFPA^{2D} code can be found in the published literature [47].

3.2. Brazilian Disc Test of Layered Rock Specimens by RFPA^{2D}

3.2.1. Numerical Layered Specimens of Brazilian Test

Numerical rock specimens with seven different dip angles of 0° 15°, 30°, 45°, 60°, 75°, and 90° were prepared, and are shown in Figure 5. The mechanical parameters of the rock material and the joint material are listed in Table 1. The loading rate was 0.0008 mm/step in the axial direction.

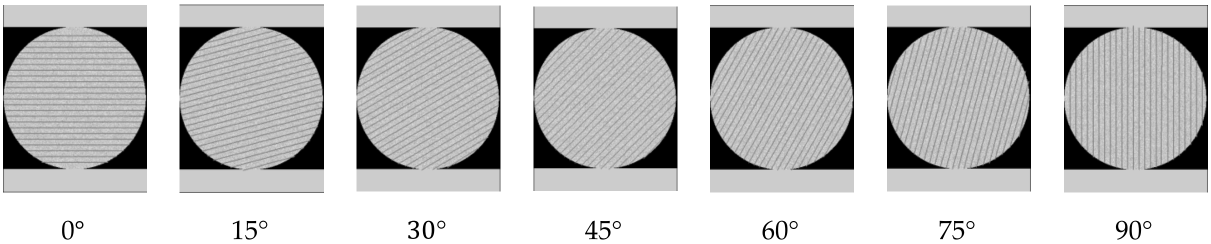

Figure 5. Numerical layered rock specimens under the Brazilian disc test.

Table 1. Elemental parameters of the rock and joint material.

Materials	Parameters	Elastic Modulus	Tensile Strength
Rock	Homogeneity index Mean value	4 50,000 MPa	4 45 MPa
Joint	Homogeneity index Mean value	3 1000 MPa	3 4 MPa

The homogeneity indices for the rock material and the joint material were 4.0 and 3.0, respectively. Because the tensile strength of the layered rocks depends on the combination of the rock material and the joint material, the strength of the transversely isotropic rock specimen with a layer dip of 90° in Liao's experiments is regarded as the tensile strength of the rock material in the present simulations, and the strength of the transversely isotropic rock specimen with a layer dip of 0° is regarded as the tensile strength of the joint material. A series of numerical tests was carried out to obtain the macro-tensile strength and the elastic modulus parameters according to Liao's experimental study [40]. The mechanical parameters of these two materials are listed in Table 1.

To obtain the mechanical parameters of these two materials, two numerical specimens made of the rock material or the joint material only were also prepared to conduct indirect tensile tests. The elastic modulus and the tensile strength of them are listed in Table 2.

Table 2. Macro-mechanical parameters of the rock and joint material.

Materials	Elastic Modulus (MPa)	Tensile Strength (MPa)
Rock	40,712.5	15.3
Joint	415.8	1.1

3.2.2. Results and Analysis

Figure 6 shows the tensile strength of the layered rock specimens under the numerical Brazilian test, which is calculated by Equation (1). The tensile strength of the layered rock specimens decreases with the increasing dip angle; the maximum tensile strength is 11.49 MPa at a dip angle of 0°, which corresponds to the direct tension strength at a dip angle of 90°. Figure 7 shows the horizontal stress at the center of the specimen vs. the vertical loading displacement. The pre-peak behavior of the specimens with different dip angles is quite similar, showing a linear elastic behavior. Figures 6 and 7 indicate that the tensile strength and loading curves of the layered rock specimens under the Brazilian test are very sensitive to the dip angle.

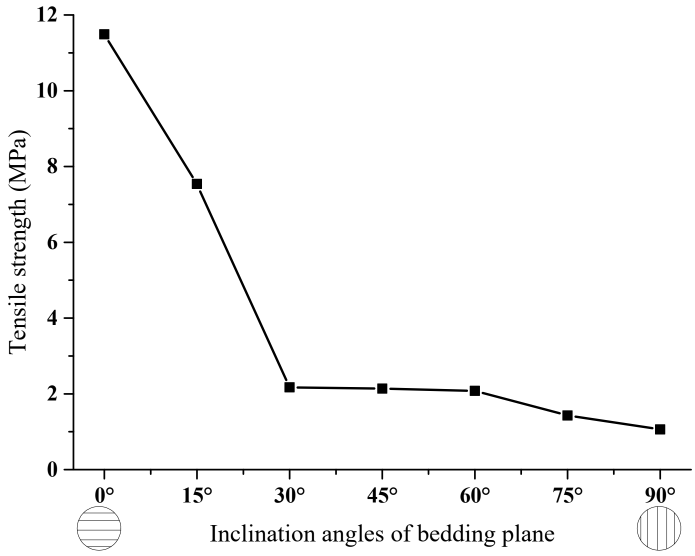

Figure 6. Tensile strength of layered rock specimens under the Brazilian test.

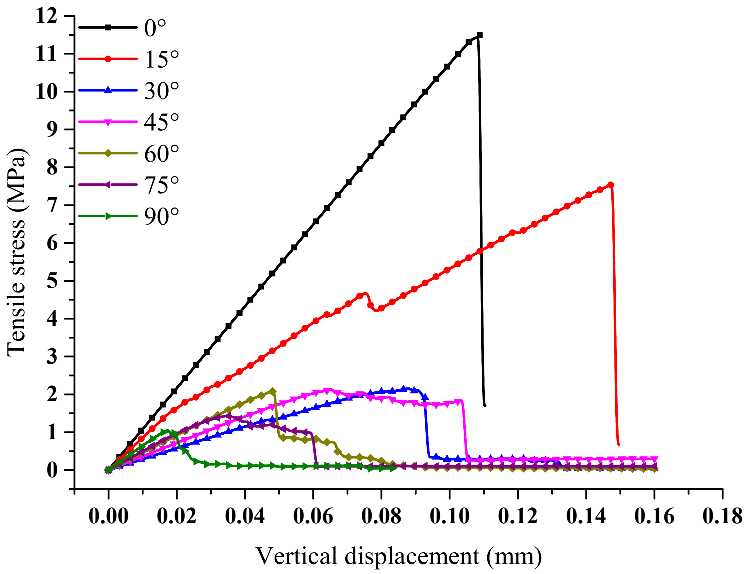

Figure 7. Horizontal stress (tensile stress) at the center of specimen vs. vertical displacement.

Figure 8 presents the failure modes of the layered rock specimens under the Brazilian test. It can be clearly seen that the failure mode of the specimen at 0° is similar to the isotropic rocks. The cracks generate at the center of the specimen, then propagate in a direction towards to the loading ends, and finally penetrate the whole specimen. After that, there are some small shear cracks near the loading ends. The main failure mechanism in this case is rock material tensile splitting. The tensile strength of the specimen at 0° is 11.49 MPa, which is similar to the tensile strength in the direct tension test (11.42 MPa) and the laboratory test (12.50 MPa). The failure modes of the specimens at 15°, 30°, and 45°. are quite complicated, and they show a mixed failure mode combining tensile splitting and shear failure. With the increasing dip angle, the shear cracks along the bedding planes increase. Shear cracks generate at the contacts of the rock material and the joint material, but they do not propagate any farther along the bedding planes. After that, the tensile cracks generate in the rock material, then propagate to shear cracks. Finally, the shear cracks and tensile cracks penetrate the specimen, which results in the specimen failure. The failure modes of the specimens at 60° and 75° are relatively simple, showing a shear failure along the bedding planes. Shear cracks generate at the contacts of the rock material and the joint material, and the cracks propagate along the bedding plane until they penetrate the whole specimen, which finally result in the specimen shear failure. The main crack does not cross the center of the specimen, and no tensile cracks are generated in the center of the disc. The failure mode of the specimen at 90° is similar to that of the specimen at 0°; the cracks generate almost in the center of the disc and propagate towards the loading ends until the cracks penetrate the whole specimen. The tensile strength of the specimen at 90° is 1.06 MPa, which is much lower than the tensile strength of the specimen at 0°. The main failure mechanism in this case is joint material tensile splitting. In conclusion, there are three main failure modes of the layered rock specimens under the Brazilian test, including tensile splitting failure, mixed tensile splitting and shear failure, and shear failure.

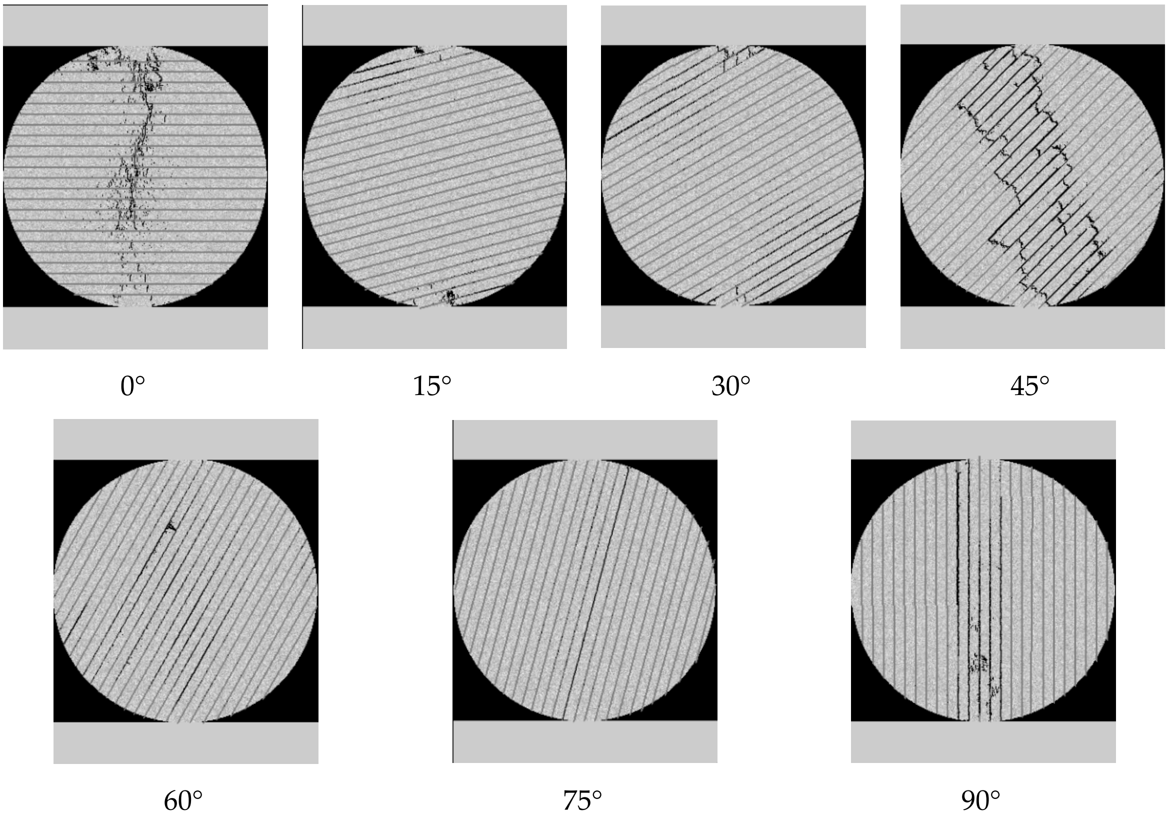

Figure 8. Failure modes of the layered rock specimens under the Brazilian test.

3.3. Direct Tension Test on Layered Rock Samples by RFPA^{2D}

3.3.1. Preparation of the Numerical Layered Specimens

Tien et al. used three model materials to prepare artificial transversely isotropic rock blocks [8]. In this study, the layered rock specimens are assumed to be made up of rock material and joint material, which determines the mechanical properties of the layered rocks. In this investigation, seven rock specimens with a dip angle, θ, of 0°, 15°, 30°, 45°, 60°, 75°, and 90°, with respect to the loading direction, are made up of the two different materials. Furthermore, some extra specimens with a layer dip angle of 80° and 85° were prepared to verify the numerical results compared with Liao's experimental study [40]. The specimen size was 200 mm × 100 mm, and it was discretized into 600 × 300 (180,000 elements) meshes.

It is much more difficult to obtain efficient satisfactory transversely isotropic rock samples in laboratory experiments. With RFPA^{2D}, it is more convenient to prepare layered rock samples with different rock materials. As shown in Figure 9, the light gray rock layers and the dark gray joints constitute the numerical specimens, respectively.

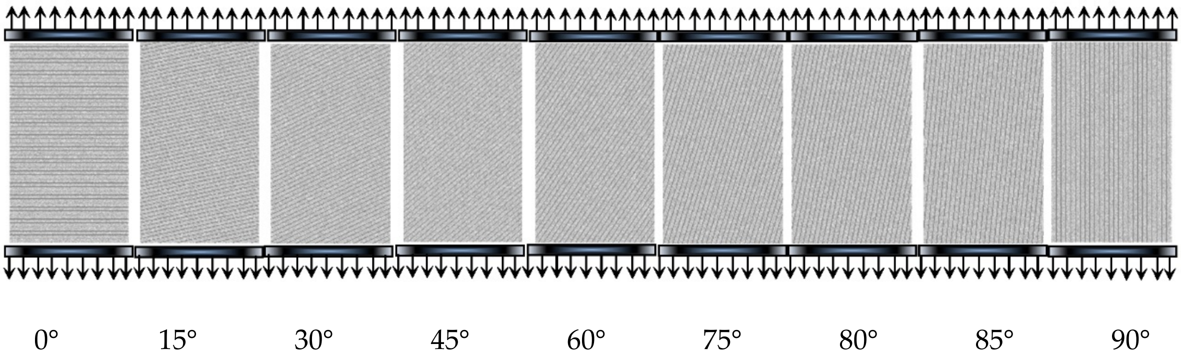

Figure 9. Layered rock specimens with different dip angles subjected to direct tension.

In all cases, the specimens underwent plane strain compression, imposed by the relative motion of the upper and lower loading plates by applying an external displacement at a constant rate of −0.0008 mm/step in the axial direction. The stress, as well as the deformation and the energy released, in each element were computed in each step during loading. The external displacement in the axial direction was slowly increased step by step.

3.3.2. Results and Analysis

The complete stress–strain relations of the layered rock specimens with dip angles, θ, of 0°, 15°, 30°, 45°, 60°, 75°, 85°, and 90° are shown in Figure 10. All stress–strain curves exhibit strong linear elasticity before the rock samples reach their peak tensile strength. The relationship between the stress and strain shows that the tensile strength increases as the dip angle increases from 0° to 90°. This means that the tensile strength is anisotropic due to the existence of weak joints. The critical strain, at the point where the specimens reach the peak tensile load, also increases when the dip angle increases from 0° to 85°. However, the critical strain of the specimen with a dip angle of 90° decreases compared with the specimen at 85°. We can consider that the critical strain may be influenced by the failure modes of the layered rock specimens.

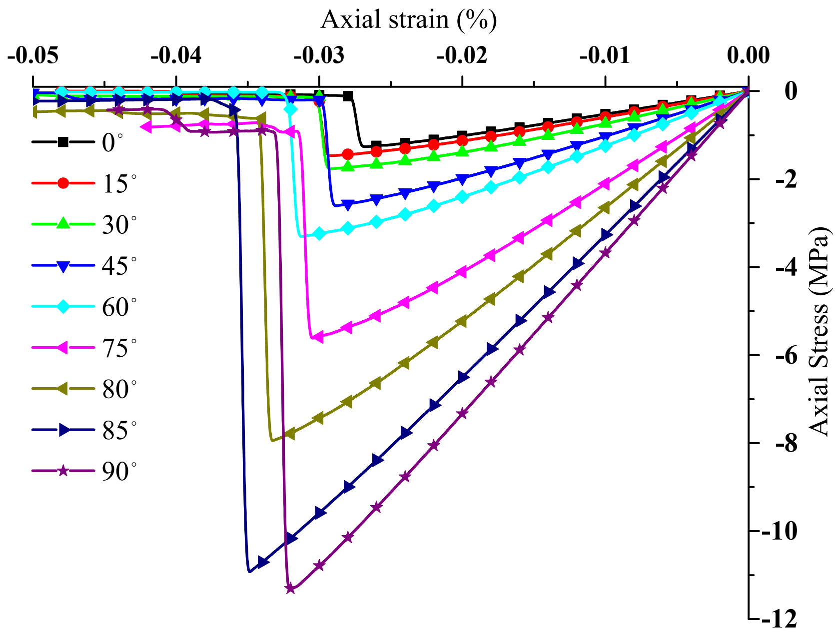

Figure 10. Complete stress–strain curves for the layered rock specimens.

The relationships between tensile strength and the tensile modulus with different dip angles are shown in Figure 11. The tensile strength of the specimen with a dip angle of 0° is very close to the tensile strength of the specimen with a dip angle of 15°. We can also see that, by varying the dip angle, the tensile modulus of the specimens follows the same trend as the tensile strength. As the dip angle increases from 0° to 90°, the tensile modulus increases gradually.

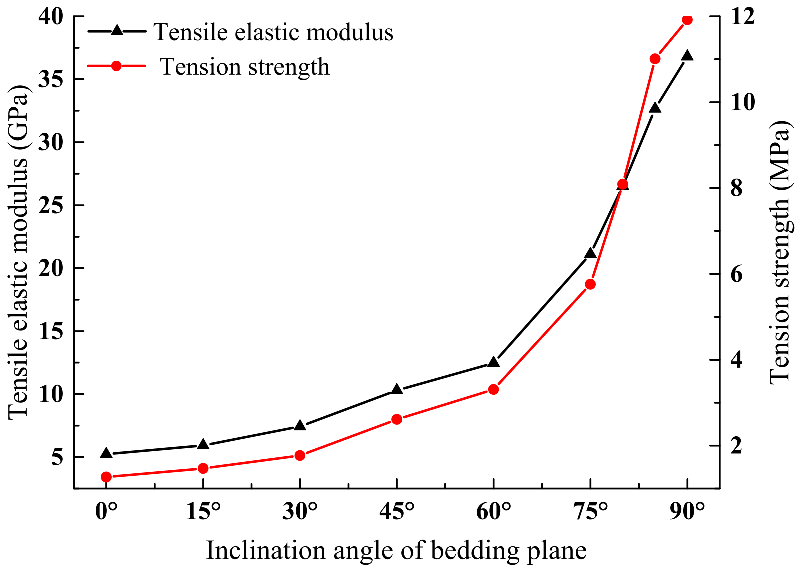

Figure 11. The tensile strength and tensile modulus of specimens with different dip angles.

It is obvious that the strength and tensile modulus of the specimens with the lower dip angles, from 0° to 15°, are closer to those of the joint material, whereas the strength and tensile modulus of the specimens with higher dip angles, from 75° to 90°, are closer to the tensile modulus of the rock material. We can conclude that the deformation behavior and tensile strength of layered rocks with lower dip angles depend on the existence of joints. However, the influence of joints on the layered rocks with higher dip angles is slight. Figure 12 shows the simulated tensile strength under direct tension, which has a good agreement with experimental results.

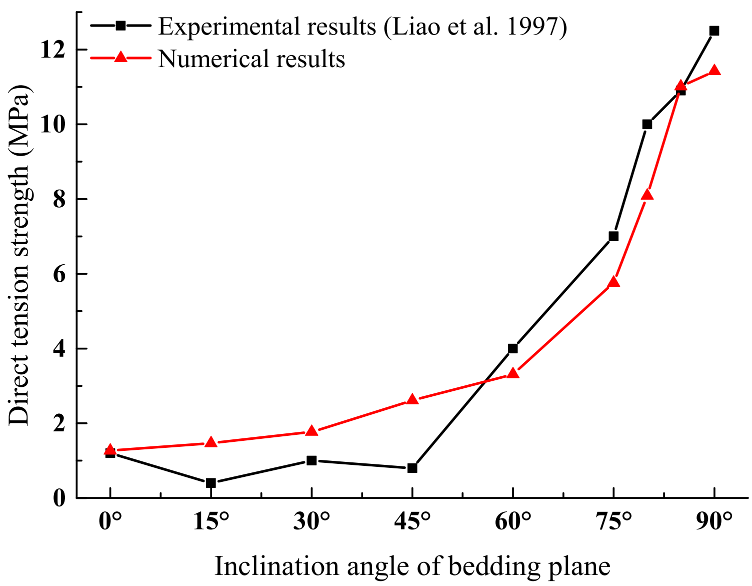

Figure 12. Tensile strength of the layered rock mass with different dip angles [40].

Figure 13 shows typical failure patterns of specimens with different dip angles. The fracture process of the specimen with a dip angle of 85° is displayed in Figure 14. The colors in Figures 13 and 14 represent the value of minimal principal stress. We can observe that the fracture of specimens with a lower dip angle, from 0° to 60°, is caused by the propagation of joints, and the fractures occur along joints from one side to the other. More than two fractures are observed in the specimens with a dip angle from 0° to 45°, whereas only one fracture can be seen along the joint from the upper-right to the lower-left corner in the specimen with a dip angle of 60°.

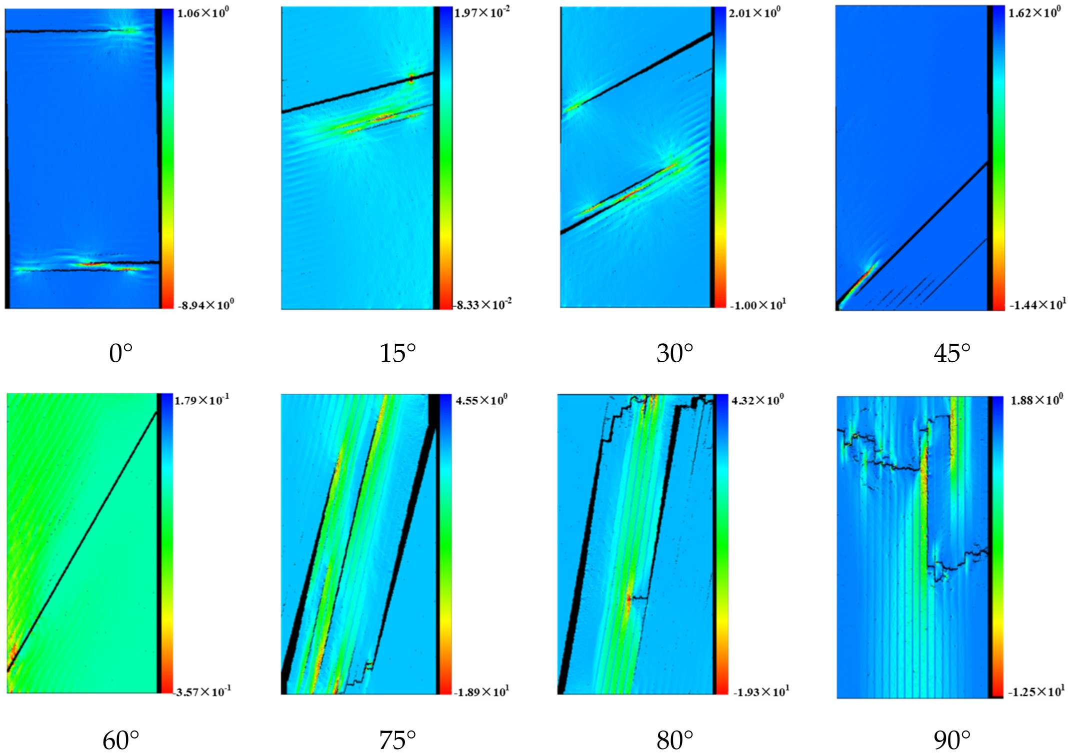

Figure 13. Fracture patterns of specimens with a layer dip angle from 0° to 80° and 90°.

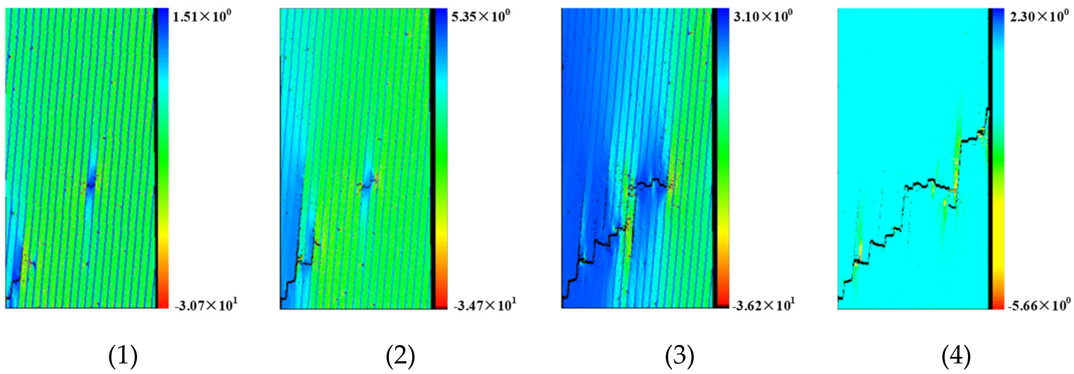

Figure 14. The failure process of the specimen with a layer dip angle of 85°.

However, for the specimens with dip angles of 75°, 80°, and 85°, fractures propagate partly along and partly through the joints. The failure plane exhibits a saw-toothed shape, and the same phenomenon was also observed in Youash's tests [39] and Liao's experiments [40]. For the specimens with dip angles of 75° and 80°, the cracks initiate along the joints from the left or right boundary, then propagate along the joints. Before they reach the other end, the new cracks initiate and propagate in the rock material perpendicular to the joints. The cracks perpendicular to the loading direction only occur near the top or the bottom end of the specimens.

For specimens with layers parallel to the tensile direction with angles of 85° and 90°, the fracture plane also exhibits a clear saw-toothed shape, but only a few parts of the failure plane occur along the foliation. The phenomenon of the saw-toothed failure plane reflects the fact that progressive failure occurs during the direct tensile tests. The progressive failure may include primary tensile cracks perpendicular to the tensile loading direction and secondary cracks parallel to the joints.

Figure 14 shows the progressive failure process of the specimen with a dip angle of 85°. It is interesting to see that the cracks do not initiate perpendicular to the loading direction in the joint material but in the rock material. They often run across many layers before beginning to propagate along the joints. The saw-toothed fracture pattern is caused by alternate propagation perpendicular to the loading direction and along the joints.

Figure 15 shows the failure patterns of sandstone of Lyons, tested in direct tension with different inclined angles by Youash in 1969 [39]. In the direct uniaxial tension tests, we can see that, when the inclined angle is less than 45°, the sandstone of Lyons mainly undergoes tensile failure along the bedding plane. The sandstone of Lyons also shows the saw-toothed fracture pattern when the inclined angle of bedding plane is greater than 45° and less than 90°. When the inclined angle of the bedding plane equals 90°, the sandstone of Lyons exhibits failure of the rock material, and the failure plane is perpendicular to the loading direction.

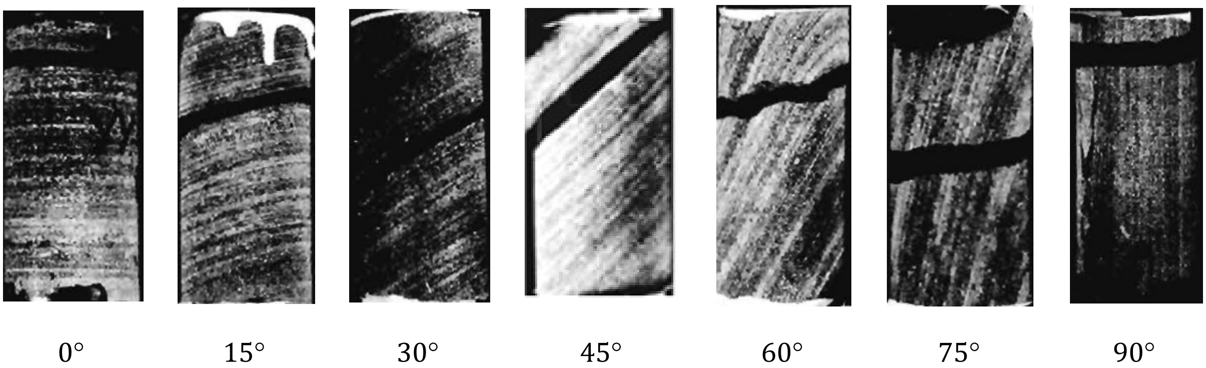

Figure 15. The failure patterns of sandstone of Lyons formation tested in direct tension [39].

The failure modes of the layered rock specimens obtained by numerical simulations under direct tension are similar to the experimental results [39,40], and the uniaxial tensile failure modes of the layered rocks can be divided into three types: (1) tensile failure along the bedding plane; (2) progressive saw-toothed failure; (3) tensile failure of rock material. The diagram of failure modes is shown in Figure 12 [40,44].

3.3.3. Failure Mechanism

Figure 16 shows the failure mechanisms of the layered rock specimens with different dip angles under direct tension, and these correspond to the three main failure modes of layered rock specimens. The layered rocks in Figure 16 is mainly composed of two materials, including rock material and joint material (bedding plane). Figure 16a illustrates that when the dip angle of the bedding plane is equal to 0°, with the increasing axial tensile load, the bedding plane will be fractured by tension while the axial tensile stress is greater than the tensile strength of the bedding plane (T_0). In this configuration, the layered rock specimen will be fractured along the bedding plane, and the tensile strength of the layered rock specimen can be expressed as $\sigma_t = \sigma_1 = T_0$.

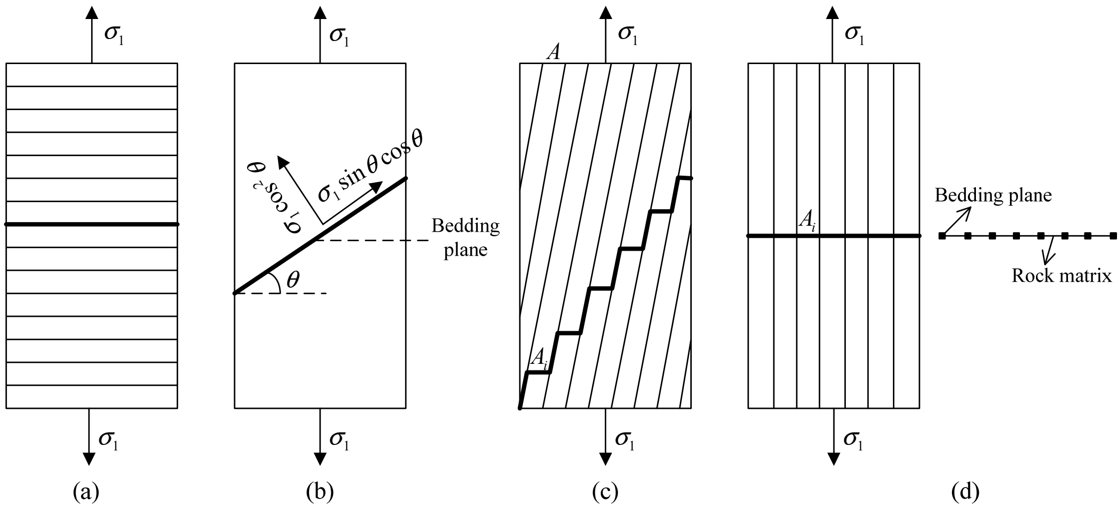

Figure 16. The tensile failure mechanism analysis of the layered rocks.

Figure 16d shows that, when the dip angle of the bedding plane is equal to 90°, with the increasing axial tensile load, the bedding plane first reaches its tensile strength, and then the bedding plane is cracked. However, in contrast to Figure 16a, the rock material is subjected to the axial tensile load at the cross section of the layered rock specimen. At the cross section, the bedding plane can be simplified as a single point when the layer thickness is small; therefore, it has little influence on the bearing capacity of the specimen while the bedding plane is first cracked. Then, as the axial tensile load increases to the tensile strength of the rock material (T_{90}), the layered rock specimen will be fractured along the cross section, resulting in tensile failure, and the failure plane is generally perpendicular to the loading direction. In this configuration, the tensile strength of the layered rock mass can be expressed as $\sigma_t = \sigma_1 = T_{90}$.

Figure 16b shows that when the dip angle of the bedding plane is greater than 0° and less than a specified angle, the layered rock mass is also fractured along the bedding plane. It can be seen in Figure 16b that the normal stress at the bedding plane is $\sigma_n = \sigma_1 \cos^2\theta$. In order to make the bedding plane fracture by tension, the normal stress at the bedding plane should be equal to the tensile strength of the bedding plane, which is expressed as $\sigma_n = T_0$. We can then obtain the tensile strength of the specimen as $\sigma_t = \sigma_1 = T_0/\cos^2\theta$. This demonstrates that the tensile strength of layered rock mass increases with the increasing dip angle.

With the increasing dip angle, the failure patterns of the layered rock specimens change. This will result in a progressive saw-toothed failure, as shown in Figure 16c. It is assumed that the area of the cross section is A, and the area of each small matrix exhibited the saw-toothed shape is A_i, so $\sigma_1 = F/A$ and $\sigma_i = F_i/A_i$. In order to make each small matrix exhibit the saw-toothed shaped cracks, the tensile stress, σ_i, needs to satisfy $\sigma_i = T_{90}$. It can then be surmised that $F_i = T_{90}A_i$. Therefore, $F = \Sigma F_i = T_{90}\Sigma A_i$, $\sigma_t = \sigma_1 = F/A = T_{90}\Sigma A_i/A$. It can be seen that, when the dip angle of the bedding plane is less than 90°, $\Sigma A_i < A$, that is to say, $\sigma_t = \sigma_1 < T_{90}$. We can see that as the layered rock mass generates the progressive saw-toothed failure, the tensile strength of the layered rock mass at this specific angle is less than the tensile strength of the layered rock specimens at a dip angle of 90°. From the point of view of geometry and elastic mechanics, this can explain the variation of tensile strength of the layered rock specimen with different dip angles of the bedding plane.

3.4. Discussion

3.4.1. Failure Modes of Layered Rock Specimens under Direct Tension Test

The main failure modes of layered rocks under the direct tension test are analyzed in Section 3.2; however, the failure modes of layered rocks highly depends on the anisotropic coefficient ($k = \frac{T_{90}}{T_0}$). If the anisotropic coefficient is less than 1 ($k < 1$), that is to say, the tensile strength of the bedding plane is stronger than the tensile strength of the rock material, it can be hypothesized that the bedding plane is the strong binding material, therefore, as the layered rock specimen is subjected to the uniaxial tensile load, the rock material will be fractured first, whatever the layer orientation is. If the anisotropic coefficient is equal to 1 ($k = 1$), which means the tensile strength of the bedding plane is the same as the tensile strength of the rock material, the tensile strength of the layered rocks may present isotropic characteristics. However, layered rocks may not only fracture along the bedding plane or the rock material due to the different elastic parameters between the bedding plane and the rock material. If the anisotropic coefficient is greater than 1 ($k > 1$), the failure modes may present as the three main patterns. In conclusion, the failure modes of layered rock specimens subjected to a direct tensile load may be greatly influenced by the anisotropic coefficient.

3.4.2. Tensile Strength of Layered Rock Specimens

For layered rocks, many Brazilian tests have been conducted to investigate the tensile behavior [48–52]. The numerical results in Section 3.2.2 shows that there are three main failure modes of layered rock specimens under the Brazilian test. Figure 17 also displays the fracture patterns of Mosel slate discs with different dip angles in laboratory tests [53]. Figure 17 shows that the layered rock specimens with different dip angles are not always fractured along the center diameter line under Brazilian tests. The failure modes are different because of the influence of the bedding planes. The typical failure patterns can be divided into three types: layer activation, central fracture, and non-central fracture. However, the precondition of Equation (1) to calculate the tensile strength of rocks should be satisfied so that Brazilian disc specimens are fractured along the center diameter line. Therefore, the tensile strength of the layered rocks calculated by Equation (1) is not reasonable, except for the specimens with dip angles of 0° and 90°, which are fractured along the center diameter line. Similar results can be found in other papers [54–57]. This demonstrates that the tensile strength of the layered rocks obtained by the Brazilian test is erroneous because of the influence of bedding planes. Specially, the tensile strength of the layered rock specimens with dip angles of 0° and 90° can be predicted by the Brazilian test because their failure modes meet the precondition of Equation (1). However, the tensile strength of the layered rock specimens obtained by the direct tension test is relatively accurate. Therefore, we suggest that the direct tension test is more suitable than the Brazilian disc test to measure the tensile strength of layered rock specimens.

0° 15° 30° 45° 60° 75° 90°

Figure 17. Fracture patterns of Mosel slate discs under different foliation-loading angles [53].

4. Modified Anisotropic Tensile Failure Criterion

4.1. Single Plane of Weakness (SPW) Criterion

Lee and Pietruszczak [43] proposed the SPW criterion of layered rocks based on Jaeger's SPW theory [9], and the SPW criterion can be given as:

$$T(\theta) = \begin{cases} \frac{T_0}{\cos^2\theta}\ 0^\circ \le \theta \le \theta^* \\ T_{90}\ \theta^* \le \theta \le 90^\circ \end{cases} \tag{3}$$

where θ^* is defined as:

$$\theta^* = \cos^{-1}\sqrt{\frac{T_0}{T_{90}}} \tag{4}$$

From Equation (3), it can be obtained that when the dip angle of the bedding plane is less than the critical angle, θ^*, the layered rock specimens in the direct tension tests are fractured along the bedding plane, which is in close compliance with the experimental results. However, when the dip angle of the bedding planes is greater than the critical angle, θ^*, the failure mode of the layered rock specimens is considered to be rock material tensile fracture under direct tension. In this situation, the tensile strength of the layered rock specimen is equal to the tensile strength of the rock material, which is inconsistent with the actual situation and the experimental results.

4.2. Modified SPW Criterion (MSPW Criterion)

To some degree, the SPW criterion can reflect the failure modes of layered rocks under direct tension. However, the failure modes may be different to the actual failure modes under the direct tension test when the dip angle is greater than the critical angle, θ^*. Therefore, based on the failure modes of the layered rocks under the direct tension test, the SPW criterion is modified in this paper.

The saw-toothed failure mode due to direct tension can be seen when the dip angle is higher, as shown in Figure 16c. The tension-fractured rock material is taken for the analysis. The rock material is not only subjected to the force generated by the normal stress, σ_1, but is also subjected to the force generated by the shear stress of the bedding plane. The rock material will be tension fractured as long as the total stress on the rock material reaches its tensile strength, T_{90}; meanwhile, the tensile strength, σ_1, of the layered rock specimen can be obtained:

$$T_{90} = \sigma_1 + 2\sigma_1 \sin^2\theta\cos\theta \tag{5}$$

$$\sigma_1 = \sigma_t = \frac{T_{90}}{1 + 2\sin^2\theta\cos\theta} \tag{6}$$

Therefore, the modified SPW (MSPW) criterion can be written as:

$$T(\theta) = \begin{cases} \frac{T_0}{\cos^2\theta}\ \ 0^\circ \le \theta \le \theta^* \\ \frac{T_{90}}{1+2\sin^2\theta\cos\theta}\ \ \theta^* < \theta \le 90^\circ \end{cases}. \tag{7}$$

where the critical angle, θ^*, is given by:

$$\theta^* \cong \arctan\left(\sqrt{\frac{T_{90}}{T_0}} - 1\right) \tag{8}$$

4.3. Verification of the MSPW Criterion

The numerical tests are based on the experiments of layered rocks carried out by Liao et al. [40]. Figure 18 shows the result comparisons between the laboratory test, numerical simulation, the Liao criterion, the SPW criterion, and the MSPW criterion.

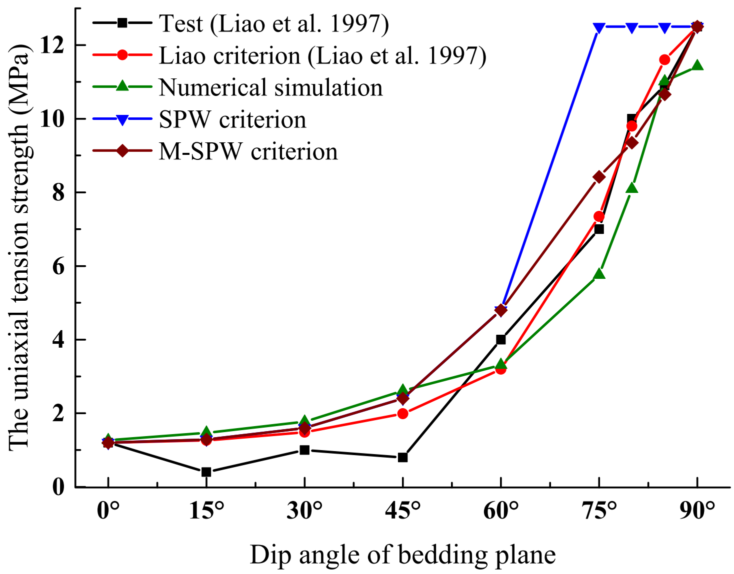

Figure 18. The result comparisons of laboratory test, simulations, and theoretical analysis [40].

Figure 18 illustrates that the results predicted by the MSPW criterion are closer to the experimental results. However, the results predicted by the SPW criterion greatly deviate from the test results at a higher dip angle. The tensile strength predicted by the Liao criterion has a small error compared with the test results as a whole, but the material constant in the Liao criterion is difficult to determine. We can also see that the numerical results simulated by RFPA^{2D} can well reflect the test results, and it is a good numerical method to simulate the failure process of rock samples under the direct tension test. By comparison, it is not difficult to find that the MSPW criterion is relatively accurate whether it reflects the uniaxial tensile failure modes of the layered rocks or predicts the uniaxial tensile strength of the layered rocks.

4.4. Determination of the Tensile Strength of Layered Rocks

Figures 3 and 17 present the failure modes of the layered rock specimens under the Brazilian test; it can be seen that the two specimens with 0° and 90° are almost fractured along the center diameter line. The experimental and numerical results clearly show that the tensile strength of the two specimens obtained by the Brazilian test are similar to the results by the direct tension test and laboratory test. This illustrates that although the tensile strength of the layered rocks obtained by the Brazilian test is controversial, the tensile strength of the two layered rock specimens of 0° and 90° obtained by the Brazilian test is reasonable.

From the expression of the MSPW criterion (Equation (7)), we can see that if the two parameters (T_0 and T_{90}) are determined, the tensile strength of the layered rocks with other dip angles can be predicted. However, the two parameters (T_0 and T_{90}) are difficult to obtain by the direct tension test, which is harder to carry out in the laboratory. Nevertheless, as we analyzed previously, the tensile strength of the layered rock specimens with dip angles of 0° and 90° (T_0 and T_{90}) can be obtained by the Brazilian test, whose results are reasonable. Thus, based on the MSPW criterion, we can simply predict the tensile strength of the layered rocks with different dip angles.

5. Conclusions

This study focuses on the tensile behavior of a transversely isotropic rock with varied layer dip angles subjected to direct and indirect tension tests. The following conclusions can be drawn:

(1) The layered rock specimens display an anisotropic mechanical behavior when subjected to direct tension load. The tensile stress–strain behavior of the layered rocks depends on the direction of the bedding planes with respect to the tensile load. However, the direct tension test of layered rocks in the laboratory needs to be studied in more depth in the future.
(2) The numerical results show that the dip angle has a significant influence on the fracture characteristics during the progressive failure, such as peak strength, failure patterns, and deformational behavior. The failure modes of the layered rock specimens are characterized by tensile failure along the bedding plane, progressive saw-toothed failure, and tensile failure of the rock material under direct tension.
(3) Based on the failure modes of the layered rocks, the SPW failure criterion is modified. The theoretical results of the modified SPW (MSPW) failure criterion show a good agreement with the experimental and the numerical results. The MSPW failure criterion can accurately describe the tensile strength when the dip angle of the bedding plane is close to 45°.
(4) Based on the MSPW criterion, a method to determine the tensile strength of the layered rocks is proposed, which can simply predict the tensile strength of the layered rocks.

Author Contributions: Conceptualization, S.J.; Data curation, J.Z.; Formal analysis, M.G.; Funding acquisition, M.G.; Investigation, M.G. and J.Z.; Methodology, Z.L.; Resources, S.J.; Software, Z.L.; Supervision, Z.L.; Writing—original draft, M.G.; Writing—review & editing, Z.L. All authors have read and agreed to the published version of the manuscript.

Funding: This research was funded by the Natural Science Foundation of Anhui Province (2108085QE208), the China Postdoctoral Science Foundation Funded Project (2021M700753), the Natural Science Research Project of Universities in Anhui Province (KJ2021A0463), and the National Natural Science Foundation of China (51779031, 41977219).

Institutional Review Board Statement: Not applicable.

Informed Consent Statement: Not applicable.

Data Availability Statement: The results reported in this study were obtained using our in-house code. The experimental data were obtained from measurements and experiments on RMT-150C. The data for producing the reported results will be made available upon request.

Conflicts of Interest: The authors declare no conflict of interest.

References

1. Donath, F.A. Strength variation and deformational behavior in anisotropic rock. In *State of Stress in the Earth Crust*; Judd, W.R., Ed.; Elsevier: Amsterdam, The Netherlands, 1964; pp. 281–300.
2. Amadei, B.; Rogers, J.D.; Goodman, R.E. Elastic constants and tensile strength of the anisotropic rocks. In Proceedings of the Fifth Congress of International Society of Rock Mechanics, Melbourne, Australia, 10–15 April 1983; Balkema: Rotterdam, The Netherlands, 1983; pp. 189–196.
3. Amadei, B. Importance of anisotropy when estimating and measuring in situ stresses in rock. *Int. J. Rock Mech. Min. Sci. Geomech. Abstr.* **1996**, *33*, 293–325. [CrossRef]
4. Gao, M.; Liang, Z.Z.; Jia, S.P.; Li, Y.C.; Yang, X.X. An equivalent anchoring method for anisotropic rock masses in underground tunnelling. *Tunn. Undergr. Space Technol.* **2019**, *85*, 294–306. [CrossRef]
5. Yagiz, S. Utilizing rock mass properties for predicting TBM performance in hard rock condition. *Tunn. Undergr. Space Technol.* **2008**, *23*, 326–339. [CrossRef]
6. Singh, T.N.; Pradhan, S.P.; Vishal, V. Stability of slopes in a fire-prone mine in Jharia Coalfield, India. *Arab. J. Geosci.* **2013**, *6*, 419–427. [CrossRef]
7. Mclamore, P.B.; Gray, K.E. The mechanical behaviour of anisotropic sedimentary rocks. *J. Eng. Ind.* **1967**, *89*, 62–76. [CrossRef]
8. Tien, Y.M.; Tsao, P.F. Preparation and mechanical properties of artificial transversely isotropic rock. *Int. J. Rock Mech. Min. Sci.* **2000**, *37*, 1001–1012. [CrossRef]
9. Jaeger, J.C.; Cook, N.G.W.; Zimmerman, R.W. *Fundamentals of Rock Mechanics*, 4th ed.; Blackwell Publishing: Malden, MA, USA, 2007.
10. Aadnoy, B.; Looyeh, R. *Petroleum Rock Mechanics: Drilling Operations and Well Design*; Gulf Professional Publishing: Oxford, UK, 2011.

11. Wu, N.; Liang, Z.Z.; Li, Y.C.; Li, H.; Li, W.R.; Zhang, M.L. Stress-dependent anisotropy index of strength and deformability of jointed rock mass: Insights from a numerical study. *Bull. Eng. Geol. Environ.* **2019**, *78*, 5905–5917. [CrossRef]
12. Guo, F.; Liang, Z.Z.; Gong, B.; Li, G. Tensile failure in stability analysis of rock and soil slopes. *Chin. J. Rock Mech. Eng.* **2017**, *36*, 3192–3205. (In Chinese)
13. Chen, Y.L.; Azzam, R.; Wang, M.; Xu, S.; Chang, L.Q. The uniaxial compressive and tensile tests of frozen saturated clay in Shanghai area. *Environ. Earth Sci.* **2011**, *64*, 29–36. [CrossRef]
14. ISRM. Suggested methods for determining tensile strength of rock materials. *Int. J. Rock Mech. Min. Sci. Geomech. Abstr.* **1978**, *15*, 99–103. [CrossRef]
15. Hobbs, D.W. Rock tensile strength and its relationship to a number of alternative measures of rock strength. *Int. J. Rock Mech. Min. Sci. Geomech. Abstr.* **1967**, *4*, 115–127. [CrossRef]
16. Li, D.Y.; Wong, L.N.Y. The Brazilian disc test for rock mechanics applications: Review and new insights. *Rock Mech. Rock Eng.* **2013**, *46*, 269–287. [CrossRef]
17. Wu, B.; Chen, R.; Xia, K. Dynamic tensile failure of rocks under static pretension. *Int. J. Rock Mech. Min. Sci.* **2015**, *80*, 12–18.
18. Bai, Q.S.; Tu, S.H.; Zhang, C. DEM investigation of the fracture mechanism of rock disc containing holes and its influence on tensile strength. *Theor. Appl. Fract. Mech.* **2016**, *86*, 197–216. [CrossRef]
19. Khosravi, A.; Simon, R.; Rivard, P. The shape effect on the morphplogy of the fracture surface induced by the Brazilian test. *Int. J. Rock Mech. Min. Sci.* **2016**, *93*, 201–209. [CrossRef]
20. Xia, K.; Yao, W.; Wu, B. Dynamic rock tensile strengths of Laurentian granite: Experimental observation and micromechanical model. *J. Rock Mech. Geotech. Eng.* **2017**, *9*, 116–124. [CrossRef]
21. Yuan, R.; Shen, B. Numerical modelling of the contact condition of a Brazilian disk test and its influence on the tensile strength of rock. *Int. J. Rock Mech. Min. Sci.* **2017**, *93*, 54–65. [CrossRef]
22. Zhang, S.W.; Shou, K.J.; Xian, X.F.; Zhou, J.P.; Liu, G.J. Fracture characteristics and acoustic emission of anisotropic shale in Brazilian tests. *Tunn. Undergr. Space Technol.* **2018**, *71*, 366–381. [CrossRef]
23. Wang, P.T.; Cai, M.F.; Ren, F.H. Anisotropic and directionality of tensile behaviours of a jointed rock mass subjected to numerical Brazilian tests. *Tunn. Undergr. Space Technol.* **2018**, *73*, 139–153. [CrossRef]
24. Barla, G.; Innaurato, N. Indirect tensile testing of anisotropic rocks. *Rock Mech.* **1973**, *5*, 215–230. [CrossRef]
25. Debecker, B.; Vervoort, A.; Napier, J.A.L. Fracturing in and around a natural discontinuity in rock: A comparison between boundary and discrete element models. In Proceedings of the 5th International Conference on Engineering Computational Technology, Las Palmas, Spain, 12–15 September 2006; p. 186.
26. Debecker, B.; Vervoort, A. A Two-dimensional discrete element simulations of the fracture behavior of slate. *Int. J. Rock Mech. Min. Sci.* **2013**, *61*, 161–170. [CrossRef]
27. Park, B.; Min, K.B. Discrete element modeling of transversely isotropic rock. In Proceedings of the 47th US Rock Mech/Geomech Symp ARMA, San Francisco, CA, USA, 23–26 June 2013; Volume 13, p. 490.
28. Dan, D.Q.; Konietzky, H.; Herbust, M. Brazilian tensile strength tests on some anisotropic rocks. *Int. J. Rock Mech. Min. Sci.* **2013**, *58*, 1–7. [CrossRef]
29. Dan, D.Q.; Konietzky, H. Numerical simulations and interpretations of Brazilian tensile tests on transversely isotropic rocks. *Int. J. Rock Mech. Min. Sci.* **2014**, *71*, 53–63. [CrossRef]
30. Liu, S.Y.; Fu, H.L.; Rao, J.Y.; Dong, H.; Cao, Q. Research on Barzilian disc splitting tests for anisotropy of slate under influence of different bedding orientations. *Chin. J. Rock Mech. Eng.* **2012**, *31*, 785–791. (In Chinese)
31. Vervoort, A.; Min, K.B.; Konietzky, H.; Cho, J.W.; Debecker, B.; Dinh, Q.D.; Fruhwirt, T.; Tavallali, A. Failure of transversely isotropic rock under Brazilian test conditions. *Int. J. Rock Mech. Min. Sci.* **2014**, *70*, 343–352. [CrossRef]
32. Chong, Z.H.; Li, X.H.; Hou, P.; Wu, Y.C.; Zhang, J.; Chen, T.; Liang, S. Numerical investigation of bedding plane parameters of transversely isotropic shale. *Rock Mech. Rock Eng.* **2017**, *50*, 1183–1204. [CrossRef]
33. Xu, G.W.; He, C.; Chen, Z.Q.; Su, A. Transversely isotropy of phyllite under Brazilian tests: Laboratory testing and numerical simulations. *Rock Mech. Rock Eng.* **2018**, *51*, 1111–1135. [CrossRef]
34. Kundu, J.; Mahanta, B.; Sarkar, K.; Singh, T.N. The effect of lineation on anisotropic in dry and saturated Himalayan schistose rock under Brazilian test conditions. *Rock Mech. Rock Eng.* **2018**, *51*, 5–21. [CrossRef]
35. Wijk, G. Some new theoretical aspects of indirect measurements of tensile strength of rocks. *Int. J. Rock Mech. Min. Sci. Geomech. Abstr.* **1978**, *15*, 149–160. [CrossRef]
36. *ASTM D3967-16*; Standard Test Method for Splitting Tensile Strength of Intact Core Specimens. ASTM International: West Conshohocken, PA, USA, 2001.
37. Aliha, M.R.M. Indirect tensile test assessment for rock materials using 3-D disc-type specimens. *Arab. J. Geosci.* **2014**, *7*, 4757–4766. [CrossRef]
38. Karaman, K.; Kesimal, A.; Ersoy, H. A comparative assessment of indirect methods for estimating the uniaxial compressive and tensile strength of rocks. *Arab. J. Geosci.* **2015**, *8*, 2393–2403. [CrossRef]
39. Youash, Y. Tension Tests on Layered Rocks. *Geol. Soc. Am. Bull.* **1969**, *80*, 303–306. [CrossRef]
40. Liao, J.J.; Tang, M.T.; Hsieh, H.Y. Direct tensile behavior of a transversely isotropic rock. *Int. J. Rock Mech. Min. Sci.* **1997**, *34*, 837–849. [CrossRef]

41. Barron, K. Brittle fracture initiation in and ultimate failure of rocks: Part II-Anisotropic rocks: Theory. *Int. J. Rock Mech. Min. Sci. Geomech. Abstr.* **1971**, *8*, 553–563. [CrossRef]
42. Nova, R.; Zaninetti, A. An investigation into the tensile behaviour of a schistose rock. *Int. J. Rock Mech. Min. Sci. Geomech. Abstr.* **1990**, *27*, 231–242. [CrossRef]
43. Lee, Y.K.; Pietruszczak, S. Tensile failure criterion for transversely isotropic rocks. *Int. J. Rock Mech. Min. Sci.* **2015**, *79*, 205–215. [CrossRef]
44. Ma, T.S.; Wu, B.S.; Fu, J.H.; Zhang, Q.G.; Chen, P. Fracture pressure prediction for layered formations with anisotropic rock strengths. *J. Nat. Gas Sci. Eng.* **2017**, *38*, 485–503. [CrossRef]
45. Ma, T.S.; Zhang, Q.B.; Chen, P.; Yang, C.H.; Zhao, J. Fracture pressure model for inclined wells in layered formations with anisotropic rock strengths. *J. Pet. Sci. Eng.* **2017**, *149*, 393–408. [CrossRef]
46. Shang, J.; Duan, K.; Cui, Y.; Handley, K.; Zhao, Z. Numerical investigation of the direct tensile behaviour of laminated and transversely isotropic rocks containing incipient bedding planes with different strengths. *Comput. Geotech.* **2018**, *104*, 373–388. [CrossRef]
47. Tang, C.A. Numerical simulation of progressive rock failure and associated seismicity. *Int. J. Rock Mech. Min. Sci.* **1997**, *34*, 249–261. [CrossRef]
48. Chen, C.S.; Pan, E.; Amadei, B. Determination of deformability and tensile strength of anisotropic rock using Brazilian tests. *Int. J. Rock Mech. Min. Sci.* **1998**, *35*, 43–61. [CrossRef]
49. Tavallali, A.; Vervoort, A. Failure of layered sandstone under Brazilian test conditions: Effect of micro-scale parameters on macro-scale behavior. *Rock Mech. Rock Eng.* **2010**, *43*, 641–653. [CrossRef]
50. Tavallali, A.; Vervoort, A. Effect of layered orientation on the failure of layered sandstone under Brazilian test conditions. *Int. J. Rock Mech. Min. Sci.* **2010**, *47*, 313–322. [CrossRef]
51. Tavallali, A.; Vervoort, A. Behaviour of layered sandstone under Brazilian test conditions: Layered orientation and shape effects. *J. Rock Mech. Geotech. Eng.* **2013**, *5*, 366–377. [CrossRef]
52. Khanlari, G.; Rafiei, B.; Abdilor, Y. An experimental investigation of the Brazilian tensile strength and failure patterns of Laminated sandstones. *Rock Mech. Rock Eng.* **2015**, *48*, 843–852. [CrossRef]
53. Tan, X.; Konietzky, H.; Fruhwirt, T.; Dan, D.Q. Brazilian tests on transversely isotropic rocks: Laboratory testing and numerical simulations. *Rock Mech. Rock Eng.* **2015**, *48*, 1341–1351. [CrossRef]
54. Cho, J.W.; Kim, H.; Jeon, C.K.; Min, K.B. Deformation and strength anisotropy of Asian gneiss, Boryeong shale, and Yeoncheon schist. *Int. J. Rock Mech. Min. Sci.* **2012**, *50*, 158–169. [CrossRef]
55. Simpson, N.D.J. An Analysis of Tensile Strength, Fracture Initiation and Propagation in Anisotropic Rock (Gas Shale) Using Brazilian Test Equipped with High Speed Video and Acoustic Emission. Master's Thesis, Norwegian University of Science and Technology, Trondheim, Norway, 2013.
56. Deng, H.F.; Zhang, X.J.; Zhang, H.B.; Wang, C.X.J.; Fang, J.C.; Xiao, Y. Analysis and discussion on Brazilian tests on layered rock tensile strength. *Rock Soil Mech.* **2016**, *37*, 309–316. (In Chinese)
57. Wang, P.T.; Yang, T.H.; Xu, T.; Yu, Q.L.; Liu, H.L. A model of anisotropic property of seepage and stress for jointed rock mass. *J. Appl. Math.* **2013**, *2013*, 420536. [CrossRef]